Available online at www.sciencedirect.com
ScienceDirect
Solid State Communications 141 (2007) 407–411
solid state communications
www.elsevier.com/locate/ssc

Structure and electrical conductivity of a novel inorganic solid electrolyte: $Na_{14.5}[Al(PO_4)_2F_2]_{2.5}[Ti(PO_4)_2F_2]_{0.5}$ (NATP)

Ying Zhang, Peng Tian, Zhengang Sun, Ziyu Liu, Yangyang Zhang, Lihong Qu, Shiyun Sang, Zhongmin Liu*

Applied Catalysis Laboratory, Dalian Institute of Chemical Physics, Chinese Academy of Sciences, 457 Zhongshan Road, Dalian, Liaoning Province, China

Received 15 January 2006; received in revised form 4 September 2006; accepted 17 November 2006 by J. Fontcuberta
Available online 12 December 2006

Abstract

A novel inorganic solid electrolyte with a layered framework structure stable up to 1043 K, $Na_{14.5}[Al(PO_4)_2F_2]_{2.5}[Ti(PO_4)_2F_2]_{0.5}$ (NATP), has been hydrothermally prepared and characterized by single-crystal and powder X-ray diffraction techniques, X-ray fluorescence (XRF) analysis, IR spectroscopic measurement, thermogravimetric and differential thermal analysis (TGA and DTA). NATP crystallizes in the acentric hexagonal space group $P\bar{3}$ with $a = 10.448(2)$, $b = 10.448(2)$, $c = 6.589(3)$ Å, $Z = 1$, containing a large number of Na^+ cations in the interlamellar space and the cavities of its framework. There are six different crystallographic Na^+ cationic sites, in which 8% Na(5) and 12% Na(6) sites are vacant. Electrical conductivity measurements show that Na^+ cations exhibit a high mobility with two domains for the electrical conductivity versus temperature.

PACS: 66.10.Ed; 61.66.Fn; 81.10.-h; 61.10.Nz

Keywords: A. Inorganic solid electrolyte; A. NATP; B. Hydrothermal synthesis; C. Crystalline structure

1. Introduction

Inorganic solid electrolytes have been widely studied during the last 30 years owing to their applications in fuel cells, ion selective membranes and electrochemical sensors [1–11]. Recently, the electrical properties of phosphates have been investigated, among which the mixed-metal phosphates with electrical conduction properties have attracted increasing attention, for their diversity of structure types and abundance of metal phosphate framework compounds [12–21]. Transition metal-containing phosphates became most attractive materials following the successful incorporation of transition metals into alumino- and gallophosphate structures in which the coordination number of metal atoms was largely observed to be greater than four due to the structure-directing role of transition metal coordination complexes. Such materials offer a great deal of scope, since they may contain metals in different valence states and/or different coordination numbers, and the anionic framework could be all oxide or oxide and fluoride [22].

This research work, for the first time, reports the successful synthesis of a new type of inorganic solid electrolyte with a 2D framework, i.e. inorganic phosphate material $Na_{14.5}[Al(PO_4)_2F_2]_{2.5}[Ti(PO_4)_2F_2]_{0.5}$ (NATP). In contrast to the well-known aluminophosphates with tetrahedrally coordinated aluminum atoms in the framework, all the aluminum atoms in NATP structure are in octahedral coordination. The NATP crystals contain larger amount of Na^+ cations (30.07 wt%) located between the interlamellar space and in the cavities of the framework. Electrical conductivity measurements show that Na^+ cations exhibit a high mobility with two domains for the electrical conductivity versus temperature. Moreover, ion-exchange experiments indicate that Na^+ cations in the crystal could be exchanged by other cations under mild conditions, which provides a possible way to enhance the ion conductivity greatly by replacing Na^+ cations with smaller cations.

* Corresponding author. Tel.: +86 411 848685510; fax: +86 411 848685510.
E-mail address: liuzm@dicp.ac.cn (Z. Liu).

0038-1098/$ - see front matter © 2006 Elsevier Ltd. All rights reserved.
doi:10.1016/j.ssc.2006.11.024

2. Experimental

2.1. Synthesis

The titled compound was hydrothermally crystallized from a mixture of titanium sulphate, aluminum nitrate, phosphoric acid, hydrofluoric acid, ethylenediamine and water with molar ratios of 1:3:16:4:3:40 and the pH value adjusted to 8.5 by adding the saturated NaOH solution. The mixture was then transferred into a stainless-steel autoclave (75 ml), heated to 463 K and kept for 7 days at this temperature. The resulting white crystals were washed several times with distilled water and dried at 373 K for 10 h.

2.2. Structural analysis

Single-crystal X-ray diffraction data were collected and analyzed on a Bruker Smart CCD diffractometer equipped with a sealed fine-focused tubular X-ray source (graphite-monochromatic Mo Kα radiation, $\lambda = 0.71073$ Å) at 293 K. 2324 reflections were measured and 950 unique ($R_{\text{int}} = 0.0420$) were used in all calculations. Final GooF = 1.133, $R1 = 0.0484$, $wR2 = 0.0987$. The structure solution and refinement were calculated with SHELXTL software package (version 6.12), using a direct method to solve the structure of the crystal, with a full-matrix least-squares refinement against F^2.

The powder X-ray diffraction patterns were recorded on a D/MAX-b X-ray diffractometer with Cu Kα radiation ($\lambda = 1.5206$ Å) with a graphite monochromator. Elemental analyses were conducted on Magix 2424 X-ray fluorescence analysis diffractometer. Thermogravimetric analyses were performed on a Perkin-Elmer 1 thermal analyzer in N_2 flow at a heating rate of 10 K/min from 323 to 1223 K. Differential thermal analysis was performed on a Perkin-Elmer DTA-7 thermal analyzer in conditioned air at a heating rate of 10 K/min from 323 to 1223 K. IR spectra were recorded on an EQUINOX 55 FTIR spectrometer (KBr pellet) at room temperature.

2.3. Electrical conductivity measurement

Electrical conductivity of the sintered disc was measured using an alternating current impedance technique. The crystals of NATP were pressed to a disc under a pressure of 60 kg/cm^2. After being sintered at 973 K for 12 h, the disc was coated with silver paint, dried at 373 K and then heated at 923 K for 1 h. The sample disc was then sandwiched between two silver plates to ensure good electrode–electrolyte contact. Electrical conductivity of the sintered disc (21 mm diameter and 1.8 mm thick) was measured from 423 to 923 K in the frequency range of 0.1 Hz–1.5 MHz by using a Solartron 1287 potentiostat and 1260 frequency-response analyzer. The entire cell assembly was placed in a tubular furnace with an accuracy of ±0.1 K.

2.4. Ion-exchange capacity

Ion-exchange experiments were carried out with 1 g NATP placed in 250 ml HNO_3 solution (pH = 1) and 250 ml $LiNO_3$ solution (0.8 mol/L) respectively, stirring at room temperature for 24 h. The replacement of Na^+ from the ion exchanger by the H^+ and Li^+ of the solution was detected by X-ray fluorescence analysis.

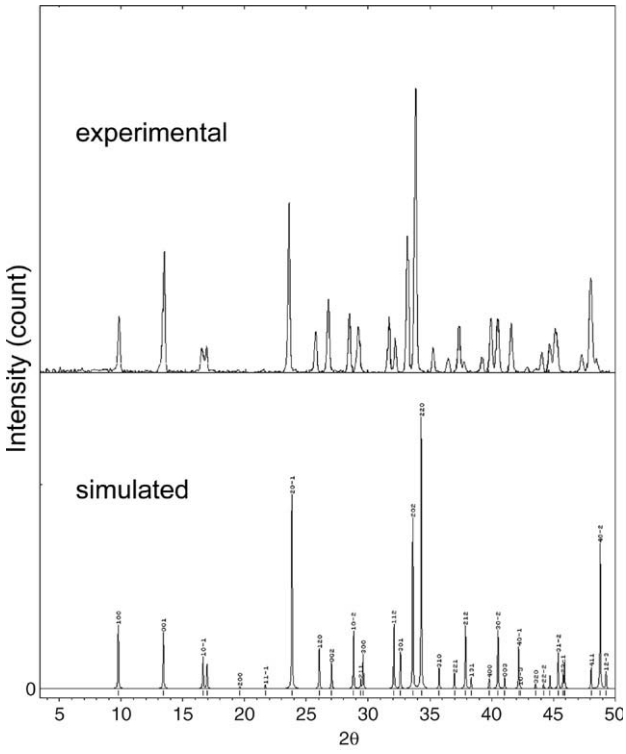

Fig. 1. The powder XRD patterns of NATP simulated on the basis of the single-crystal structure by the software PowderX.

3. Results and discussion

3.1. Synthesis and characterization

The formation of NATP crystals was observed to be sensitive to the pH. Some crystal impurities will appear in the resulting sample when pH is in the range of 9–10 or 7–8, and NATP could not be obtained when pH > 10 or pH < 7. Inspection under a microscope revealed that the crystals of NATP are homogeneous with hexagonal prisms when the synthesis is under optimized condition (pH = 8.5). XRF elementary analysis of pure NATP crystals show that the atomic ratios are Na/P = 2.50, Al/P = 0.42, Ti/P = 0.08 and F/P = 1.17 in the solid, roughly in agreement with theoretical values of 2.42, 0.42, 0.08 and 1.

The powder XRD pattern of NATP together with the simulation on the basis of the single-crystal structure is presented in Fig. 1. The reflection positions of the two patterns are essentially identical, confirming that the reaction product is a crystallographically pure phase. The differences in reflection intensities are probably due to preferred orientation in the powder crystals.

DTA curve reveals a sharp endothermic peak around 1061 K (starting point at 1043 K) while TGA curve does not appear to have any mass loss over the range of 323–1173 K. Both the TGA and DTA results indicate the high thermal stability of NATP crystals. On the IR spectrum, no bands could be found

Table 1
Structural data and refinement for NATP crystal

Empirical formula	$Al_{2.5}F_6Na_{14.5}O_{24}P_6Ti_{0.5}$
Formula weight	1108.57
Temperature	293(2) K
Wavelength	0.71073 Å
Crystal system	Trigonal
Space group	$P\bar{3}$
Unit cell dimensions	$a = 10.448(2)$ Å $\alpha = 90°$
	$b = 10.448(2)$ Å $\beta = 90°$
	$c = 6.589(3)$ Å $\gamma = 120°$
Volume	622.9(3) Å^3
Z	1
Calculated density	2.955 mg/m^3
Absorption coefficient	1.081 mm^{-1}
F(000)	539
θ range for data collection	2.25° to 27.49°
Limiting indices	$-13 \le h \le 6, -9 \le k \le 10, -8 \le l \le 8$
Reflections collected	2324
Independent reflections	950 [$R_{(int)} = 0.0420$]
Refinement method	Full-matrix least-squares on F^2
Data/restraints/parameters	950/0/87
Goodness-of-fit on F^2	1.133
Final R indices [$I > 2\sigma(I)$]	$R1 = 0.0484$, $wR2 = 0.0987$
R indices (all data)	$R1 = 0.0799$, $wR2 = 0.1069$
Extinction coefficient	0.002(2)
Largest diff. peak and hole	0.517 and $-0.500e$ Å^{-3}

from 4000 to 1100 cm^{-1}, which implies there are no crystallographic water molecules and hydroxyl groups in NATP crystals. The bands resulting from the phosphate tetrahedron stretching vibrations appear in the range of 1200–970 cm^{-1}, while the bands between 620 and 500 cm^{-1} could be assigned to the phosphate tetrahedron bending vibrations. These IR results exclude the existence of $-NH_2$ and $-OH$ groups in the crystal, which agrees well with the single-crystal structure analysis.

It is interesting to note that although ethylenediamine could not be observed in the crystals, it seems that the addition of ethylenediamine is necessary for obtaining the large single-crystals during the synthesis.

3.2. Structural characterization

Single-crystal X-ray diffraction analyses reveal that NATP crystallizes in the acentric hexagonal system with $P\bar{3}$ space group. The crystallographic data and details of the data collection and refinement are listed in Table 1.

ORTEP view of the structure of NATP along [001] direction is shown in Fig. 2. The Al or Ti atom is octahedrally coordinated by two fluorine atoms, four oxygen atoms from four PO_4 units. The bond distance of Al/Ti–O ranges from 1.874(3) to 1.899(3) Å, and Al/Ti–F distance is 1.831(2) Å. The P atom is tetrahedrally coordinated with four oxygen atoms, two of which are shared with two AlO_4F_2/TiO_4F_2 octahedra. The P–O length ranges from 1.510(3) to 1.546(3) Å and O–P–O angles lie between 105.40(15)° and 112.47(16)°. Ti–O–Ti, Al–O–Al and P–O–P bondings could not observed in the structure. The covalent radii of each element are R(O) = 0.660 Å, R(F) = 0.640 Å, R(Na) = 1.860 Å, R(Al) = 1.250 Å, R(Ti) = 1.450 and R(P) = 1.100 Å respectively. The

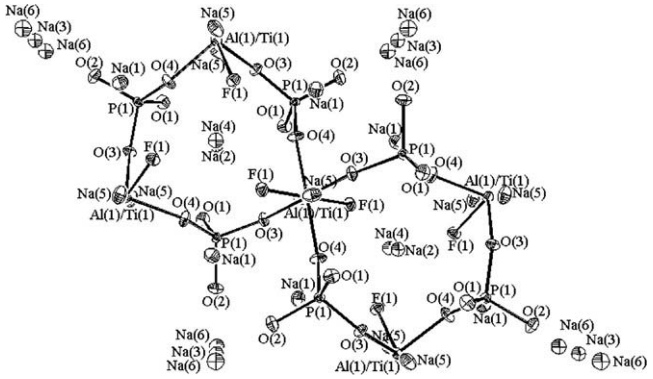

Fig. 2. ORTEP view of the structure of NATP along the [001] direction.

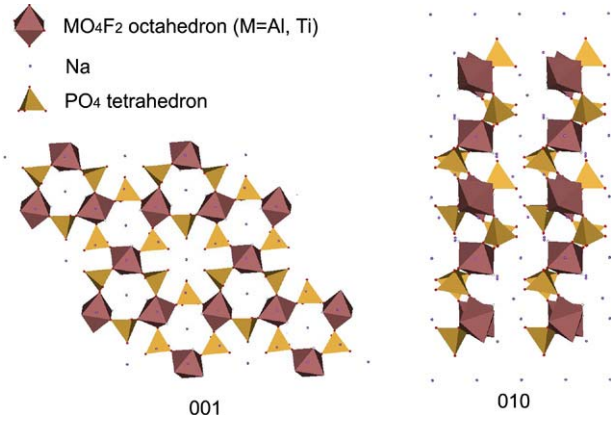

Fig. 3. Polyhedral representation of the structure of NATP.

asymmetric unit of the structure contains 14.5 nonequivalent sodium atoms occupying six different crystallographic sites in which 2% Na(1), 8% Na(5) and 12% Na(6) sites are vacant, 24 oxygen atoms occupying four different crystallographic sites, 2.5 aluminum atoms and 0.5 titanium atoms occupying one crystallographic site, 6 phosphorus atoms occupying one crystallographic site and 6 fluorine atoms occupying one crystallographic site. Of six different crystallographic sodium atoms, Na(5) and Na(6) sites are located in interlamellar space and Na(4) site is the nearest neighbor of Na(5). Of four different crystallographic oxygen atoms, O(3) and O(4) are coordinated with P(1) and Al(1)/Ti(1) forming parallel 6-MR channels and 12-MR channels along the c axis.

Polyhedral representation of the structure is illustrated in Fig. 3. A negatively charged 2D layered framework is constitutive of PO_4 tetrahedral units linked by corners to MO_4F_2 (M = Al, Ti) octahedral units, where each PO_4 tetrahedron shares two corners with two different MO_4F_2 octahedrons and each MO_4F_2 octahedron is linked to four PO_4 groups by corners. Na^+ cations are located in the interlamellar space and in the cavities of framework.

3.3. Electrical conductivity

The electrical conductivity of NATP, σ, was derived from the resistance values (Table 2). The conductivity data were represented by Arrhenius relation, given as: $\sigma = \sigma_0 \exp(-E_a/KT)$, in which σ_0 is a pre-exponential factor,

Table 2
Electrical conductivity (σ) of NATP

T (K)	R (Ω)	σ (Ω^{-1} cm^{-1}) $\times 10^5$
423	1130.33	4.60
473	523.62	9.93
523	295.43	17.60
573	161.48	32.20
623	89.49	58.10
673	48.59	106.98
723	26.82	193.87
773	18.31	283.97
823	13.76	3787.87
873	9.81	530.02
923	7.08	734.40

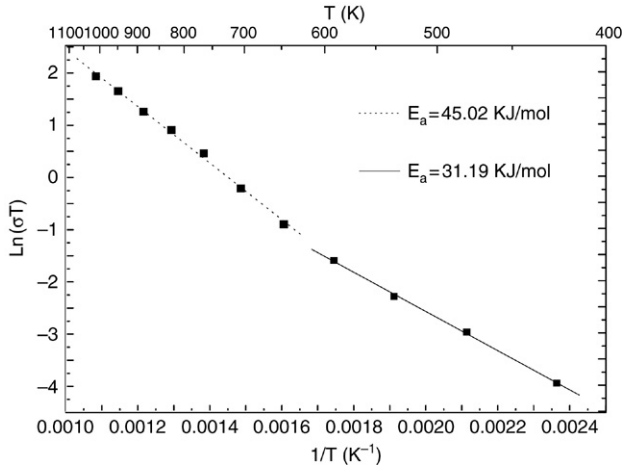

Fig. 4. Arrhenius plot Ln σT versus $1/T$ showing a discontinuity in the slope of the curve.

E_a, K and T represent the apparent activation energy for conduction process, Boltzmann's constant and the absolute temperature, respectively.

The Arrhenius plot of NATP conductivity (Fig. 4) evidences two regimes of conductivity. The first one below 600 K is characterized by an activation energy $E_a = 31.19$ kJ/mol and a conductivity of 4.60×10^{-5} Ω^{-1} cm^{-1} at 423 K, whereas the second one, above 600 K shows a much larger activation energy $E_a = 45.02$ kJ/mol and conductivity $\sigma(923\ \text{K}) = 7.34 \times 10^{-3}$ Ω^{-1} cm^{-1}. Two models could explain this particular phenomenon. In the first assumption, one can admit that the electronic contribution to the conductivity in this phase is weak, due to the fact that the MO_4F_2 (M = Al, Ti) octahedra are all separated by PO_4 tetrahedra. Thus the sodium mobility would be the main cause of conductivity. The single-crystal X-ray diffraction analysis reveals that of six different crystallographic sodium atoms 2% Na(1), 8% Na(5) and 12% Na(6) sites are vacant in which Na(5) and Na(6) sites are located in the interlamellar space. At lower temperature ($T < 600$ K), the neighboring Na(5) and Na(6) can reside in the vacancies and migrate from site to site along c axis (see Fig. 5) due to their lower activation energy leading to 1D conductivity. This 1D-conductivity corresponds to the first regime with lower activation energy 31.19 kJ/mol. At higher temperature ($T > 600$ K), the Na(4) cations can move toward the neighboring Na(5) site and Na(6) site, leading together with the mobility

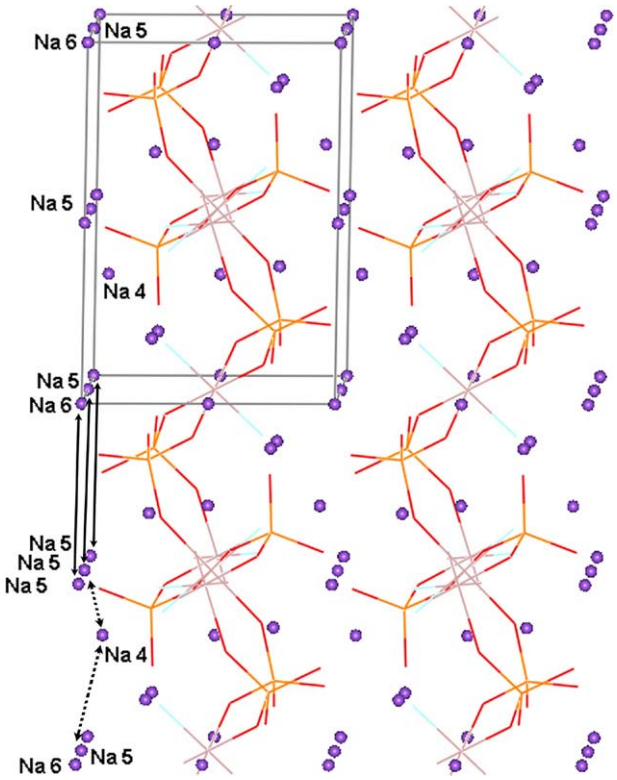

Fig. 5. The sodium layer and possible displacements of the cations. Na(5) and Na(6) can jump into the ion vacancies of Na(5) sites and Na(6) sites (full arrows), which correspond to the 1D conduction. Then at higher temperature the Na(4) can also jump to the empty Na(5) sites and Na(6) sites (dotted arrow) which corresponds to the 2D conduction.

of Na(5) and Na(6) to a 2D cationic conductivity. This second step requires higher activation energy due to the larger steric hindrance and the bottleneck created by facing oxygen atoms. In the second assumption, the 1D and 2D ionic conduction of Na^+ cations described above cannot be dissociated and are predominant at low temperature, and are consequently responsible for the first regime ($T < 600$ K), where the electronic contribution to the conductivity may be small, or even negligible. In contrast, in the second regime ($T > 600$ K) the electronic conductivity would largely predominate over the cationic conductivity, due to the fact that energy is sufficient to allow the delocalization of electrons between the MO_4F_2 (M = Al, Ti) octahedra, through PO_4 tetrahedra by tunnel effects.

3.4. Ion-exchange capacity

Ion-exchange experiments show that NATP is an excellent ion-exchanger for H^+ and Li^+. Under mild conditions (room temperature), the ion-exchange capacities of H^+ and Li^+ are as high as 12.74 and 4.51 mequiv/g, which indicates most Na^+ of NATP can be replaced and provides a chance to enhance the ion conductivity of NATP greatly by replacing Na^+ cations with smaller cations.

Preliminary result of Li-NATP exhibits an electrical conductivity of 0.147 Ω^{-1} cm^{-1} at 923 K. The valve is obviously greater than that of NATP measured at the same condition and confirms our above speculation.

4. Conclusion

In summary, a novel inorganic solid electrolyte NATP was successfully synthesized with hydrothermal method and its crystal structure was determined with single-crystal X-ray diffraction data. The crystals are with negatively charged 2D layered framework constructed by PO_4 tetrahedral units linked by corners to MO_4F_2 (M = Al, Ti) octahedral units. Abundant Na^+ cations are located in the interlamellar space and the cavities of the framework, which are highly mobile, and two domains are observed following the temperature according to electrical conductivity measurements. Moreover, ion-exchange experiments indicate that Na^+ cations in the crystal could be exchanged by H^+ and Li^+ with high ion-exchange capacity under mild conditions like room temperature, which provides a chance to enhance the ion conductivity by replacing Na^+ cations with smaller cations.

Supplementary material

The supplementary material concerning the crystal structure determination has been sent to Fachinformationszentrum Karlsruhe, D-76344 Eggenstein-Leopoldshafen, Germany, as supplementary material No. CSD-415736, and can be obtained by contacting FIZ.

Acknowledgements

The authors would like to thank Dr. Zhonghe Bi, Guangfeng Tu and Prof. Mojie Cheng (Laboratory of New Energy Resources, Dalian Institute of Chemical Physics, CAS) for their assistance with the electric experiments.

References

[1] B.B. Owens, J. Power Sources 90 (2000) 2.
[2] C.-Y. Sun, K.-Z. Fung, Solid State Commun. 123 (2002) 431.
[3] T. Ishii, Solid State Commun. 108 (1998) 513.
[4] C. Ouyang, S. Shia, Z. Wanga, X. Huanga, L. Chen, Solid State Commun. 130 (2004) 501.
[5] O. Bidault, S. Fossier, J. Mangin, P. Strimer, A. Yelisseyev, L. Lsaenko, S. Lobanov, Solid State Commun. 121 (2002) 207.
[6] J.-H. Park, Solid State Commun. 123 (2002) 291.
[7] H.K. Shin, Solid State Commun. 128 (2003) 131.
[8] J.-H. Park, B.-C. Choib, J.-B. Kim, Solid State Commun. 130 (2004) 533.
[9] K. Yamada, K. Kumano, T. Okuda, Solid State Ion. 176 (2005) 823.
[10] V. Legagneur, Y. An, A. Mosbah, R. Portal, A. Le Gal La Salle, A. Verbaere, D. Guyomard, Y. Piffard, Solid State Ion. 139 (2001) 37.
[11] K. Horchani-Naifer, M. Férid, Solid State Ion. 176 (2005) 1949.
[12] S. Ikeda, T. Kondo, S. Kato, K. Ito, K. Nomura, Y. Fujita, Solid State Ion. 79 (1995) 354.
[13] Y. Xu, S. Feng, W. Pang, Mater. Lett. 91 (1996) 499.
[14] M. Sugantha, U.V. Varadaraju, Solid State Ion. 95 (1997) 201.
[15] J. Wang, J. Wei, Y. Liu, X. Yin, X. Hu, Z. Shao, M. Jiang, Prog. Cryst. Growth Charact. 40 (2000) 3.
[16] S. Tamura, N. Imanaka, G. Adachi, Solid State Ion. 139 (2001) 153.
[17] K. Takada, M. Tansho, I. Yanase, T. Inada, A. Kajiyama, M. Kouguchi, S. Kondo, M. Watanabe, Solid State Ion. 139 (2001) 241.
[18] N. Dridi, A. Boukhari, J.M. Réau, Mater. Lett. 50 (2001) 302.
[19] K. Takada, K. Fujimoto, T. Inada, A. Kajiyama, M. Kouguchi, S. Kondo, M. Watanabe, Appl. Surf. Sci. 189 (2002) 300.
[20] S. Tamura, N. Imanaka, G. Adachi, Solid State Ion. 154–155 (2002) 767.
[21] A. Leclaire, V. Caignaert, B. Raveau, Solid State Sci. 7 (2005) 109.
[22] A.K. Cheetham, G. Férey, T. Loiseau, Angew. Chem. Int. Ed. 38 (1999) 3268.